# Identification of Semiconductor Defects through Constant-Fermi-Level *Ab Initio* Molecular Dynamics: Application to GaAs

Assil Bouzid and Alfredo Pasquarello

*Chaire de Simulation à l'Echelle Atomique (CSEA), Ecole Polytechnique Fédérale de Lausanne (EPFL), CH-1015 Lausanne, Switzerland*

We show that constant-Fermi-level *ab initio* molecular dynamics can be used as a computer-based tool to reveal and control relevant defects in semiconductor materials. In this scheme, the Fermi level can be set at any position within the band gap during the defect generation process, in analogy to experimental growth conditions in the presence of extra electrons or holes. The scheme is illustrated in the case of GaAs, for which we generate melt-quenched amorphous structures through molecular dynamics at various Fermi levels. By a combined analysis which involves both the atomic structure and a Wannier-function decomposition of the electronic structure, we achieve a detailed description of the generated defects as a function of the Fermi level. This leads to the identification of As—As homopolar bonds and Ga dangling bonds for Fermi levels set in the vicinity of the valence band. These defects convert into As dangling bonds and Ga—Ga homopolar bonds, as the Fermi level moves toward the conduction band. This demonstrates a computer-aided procedure to identify semiconductor defects in an unbiased way.

## I. INTRODUCTION

The microelectronics industry has long relied upon silicon as a substrate material. This material can be easily doped with both donors and acceptors, allowing the realization of both *n*-type and *p*-type field-effect transistors. Silicon has been particularly attractive because of its native oxide $SiO_2$, which gives rise to well-passivated interfaces and good dielectric behavior. However, further scaling of this system is prevented due to the fundamental limits associated with quantum tunneling [1,2]. This has led to a vast search for alternative classes of dielectrics and eventually of substrate semiconductors. In particular, increasing attention has recently been devoted to III-V semiconductor materials, which offer higher carrier mobilities compared to silicon [3–5]. However, their integration in metal-oxide-semiconductor field-effect transistors [6–8] is hampered by the formation of performance-degrading defects at their interfaces with other materials [9–11]. Finding suitable ways to deal with undesired defects is a general issue that often needs to be overcome upon the introduction of novel materials in electronic devices.

The identification of the underlying active defects and guidance toward their neutralization remain, to a large extent, inaccessible experimentally. Therefore, it is natural to resort to computational simulation techniques to achieve insight into possible defect structures. Current approaches for identifying defects consist of educated guesses based on physical intuition or are issued from trial-and-error procedures. Many candidate defect structures are first imagined and then realized through suitable models, in the attempt to match the available experimental characterization. In the absence of such a characterization, the selection process generally rests on the sole calculation of formation energies. However, such a procedure does not correspond to an inclusive search and the identification of the targeted defects is not guaranteed. Furthermore, the calculated energetics might be flawed by the consideration of inappropriate structural models. Given these premises, there is a growing need for the development of computer-aided simulation approaches for identifying and controlling electrically active semiconductor defects, which would not be subject to human bias.

It is suggestive to acquire inspiration from experimental studies, in which the concentration of point defects in semiconductors has been adjusted by manipulating the Fermi level during growth [12–15]. The Fermi level is experimentally controlled by inducing excess carriers through above-band-gap UV illumination. This experimental technique shows analogies with molecular dynamics simulations performed at a constant Fermi energy [16,17]. In this computational approach, the system is allowed to exchange electrons with an external potentiostat set at a prefixed-target Fermi energy. Applied to redox reactions in aqueous solution, this technique leads to the successful determination of the reaction paths and the associated redox levels [17]. Depending on the position of the prefixed Fermi level in the band gap, the system could be brought to promote the formation of the reactants or of the products. It is of interest to apply this approach to the study of semiconductor defects in the same spirit as realized in the experiments discussed above [12–15]. Defect charge transition levels separate energy ranges in the band gap, in which the defect stabilizes in different charge states. Hence, setting the Fermi level within a given energy range of the

band gap should lead at equilibrium to the formation of the defect in the corresponding charge state. The use of molecular dynamics facilitates the realization of such equilibrium conditions through thermal annealing.

In this work, we explore the possibility of using the computational framework of *ab initio* molecular dynamics at a constant Fermi level as a computer-aided tool to reveal and identify semiconductor defects. This technique offers the potential of generating majority defects in varying charge states, depending on the position of the Fermi level in the band gap. Charged defect states are allowed to be visited owing to the possibility of exchanging electrons with an external reservoir at a prefixed potential. In addition, this technique is free from human bias and may lead to the identification of defect structures which are not necessarily known *a priori*. To demonstrate the applicability of this scheme, we here focus on GaAs, a well-studied prototypical III-V semiconductor. In particular, a large body of density-functional calculations has contributed to providing a detailed description of possible defects in GaAs and at its interfaces with other materials [18–34]. Noticeably, an amphoteric defect has been suggested to be responsible for Fermi-level pinning [27,31,35,36]. For Fermi energies below the pinning level, the defect occurs in the form of a homopolar As—As bond. When the Fermi raises above the pinning level, the defect captures two electrons and transforms into two doubly occupied dangling bonds (DBs) on As atoms. This defect has been demonstrated to occur in a variety of GaAs systems, including surfaces [27], interfaces [27,35], and amorphous phases [31]. In particular, we here focus on the amorphous phase of GaAs, which represents a suitable model for bonding arrangements at interfaces of the parent crystalline semiconductor. In the amorphous phase, the occurrence of homopolar As—As bonds and As DBs has already been demonstrated in both experiments [37,38] and molecular dynamics simulations [39–41]. The constant-Fermi-level *ab initio* molecular dynamics technique is expected to reveal the occurrence of this defect and of its transformation, even in the absence of any prior knowledge. Consequently, the structure of amorphous models generated by melt-quench procedures would be highly influenced by the position of the fixed Fermi level. In particular, we demonstrate that the application of our technique to *n*-type or *p*-type semiconductors can lead to model systems with different structural properties.

The present paper is organized as follows. In Sec. II, we provide a description of the computational methodology employed in this work. Section III is devoted to the simulation protocol used to generate amorphous models of GaAs at a constant Fermi level. Our main results are given in Sec. IV. The analysis is based on both the atomic structure (Sec. IV A) and a Wannier-function decomposition of the electronic structure (Sec. IV B). Section V is devoted to the discussion of the defect concentrations as a

function of the Fermi level. The conclusions of our work are drawn in Sec. VI.

## II. COMPUTATIONAL METHODS

In this work, the electronic structure is described in the framework of density-functional theory within the generalized gradient approximation due to Perdew, Burke, and Ernzerhof [42]. The core-valence interactions are described by norm-conserving pseudopotentials according to the prescription of Troullier and Martins [43]. The wave functions of the valence electrons are expanded in a plane-wave basis set defined by a kinetic energy cutoff of 40 Ry. The Brillouin zone is sampled at the $\Gamma$ point. Our simulations are performed on a system containing $N = 64$ atoms (32 Ga and 32 As) in a periodically repeated cubic cell of size 11.54 Å, corresponding to a density $\rho = 5$ g/cm$^3$. This density lies within the experimental range 4.98–5.11 g/cm$^3$ [44–46]. We perform Born-Oppenheimer molecular dynamics using a time step of $\Delta t = 0.48$ fs to integrate the equations of motion. The control of the temperature is ensured through a velocity rescaling method.

In order to control the Fermi level during the simulation, this system is connected to an external potentiostat at a fixed potential $\bar{\epsilon}_F$ acting like an external electron reservoir. Hence, the electronic charge $N_e$ is considered as a dynamical variable having a fictitious mass $M_e$. In this way, the extended system, which comprises the physical system and the external electron reservoir, is driven by the grand canonical potential: $\Omega = E^{\mathrm{tot}}(r_i, N_e) - N_e\bar{\epsilon}_F$, where $E^{\mathrm{tot}}(r_i, N_e)$ represents the total energy of the considered system and $N_e\bar{\epsilon}_F$ the energy corresponding to $N_e$ electrons in the external reservoir [16,17]. Consequently, this formulation defines the forces acting on the atoms and the electronic charges, which are given by

$$F_i = -\frac{\partial E^{\mathrm{tot}}(r_i, N_e)}{\partial r_i} \quad \text{and} \quad F_e = -(\epsilon_F - \bar{\epsilon}_F), \quad (1)$$

where $\epsilon_F$ is the instantaneous Fermi energy. $F_e$ drives electrons into the system when $\epsilon_F$ is lower than $\bar{\epsilon}_F$ and drives electrons into the reservoir in the opposite case. The average of the instantaneous Fermi energy $\epsilon_F$ then corresponds to the preset $\bar{\epsilon}_F$. The dynamical equations for the charge evolution read

$$\dot{N}_e = \frac{P_e}{M_e} \quad \text{and} \quad \dot{P}_e = F_e = -(\epsilon_F - \bar{\epsilon}_F), \quad (2)$$

where $P_e$ is a fictitious momentum associated with the dynamical variable $N_e$. Upon the exchange of electrons with the reservoir, the charge neutrality in the supercell is ensured by the use of a uniform neutralizing background, as is customary in the study of charged defects in periodically repeated supercells [47]. Further details about the implementation of this technique can be found in Ref. [17].

In practice, we set the fictitious electronic mass to $M_e = 1000$ a.u. The temperature of the electronic charge $T_c$ is controlled by a velocity rescaling method and is set to 30 K. We use Gaussian-smeared occupations with widths of at most 0.13 eV to prevent numerical instabilities associated with the use of fractional occupations.

## III. AMORPHOUS MODEL GENERATION AT A CONSTANT FERMI LEVEL

We use the melt-quenching technique to generate our amorphous samples starting from an initial crystalline structure of GaAs. First, the initial configuration is disordered through annealing at $T = 2500$ K for a duration of 6 ps, thereby allowing for significant diffusion of both species until the memory of the initial configuration is lost. Second, the system is gradually quenched to $T = 1600$ K within 10 ps through a stepwise decrease of the temperature. We carry out a sufficiently long annealing at $T = 1600$ K for a duration of 25 ps to ensure a good diffusion in the liquid state. This state is used as the parent system for all the amorphous models generated in this work. The final amorphous structure is achieved through a quench, which gradually lowers the temperature according to the protocol: $T = 1100$ K for 10 ps, $T = 800$ K for 13 ps, $T = 500$ K for 10 ps, and $T = 300$ K for 17 ps, as graphically illustrated in Fig. 1. Statistical averages are collected over the last 10 ps of the trajectory at 300 K.

This first amorphous model is generated without the use of the constant-Fermi-level technique and is to be considered as the neutral reference system. To run *ab initio* molecular dynamics at a constant Fermi energy $\bar{\epsilon}_F$, it is required to determine the range of variation of $\bar{\epsilon}_F$ within the band gap. We therefore determine the band-edge positions of the reference amorphous model by inspecting the calculated density of electronic states (Fig. 2). The inset in Fig. 2 gives the time evolution of the highest occupied
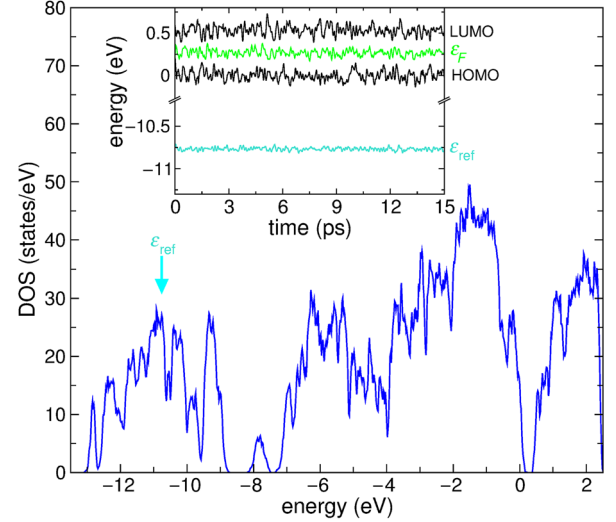


FIG. 2. Electronic density of states (DOS) for the reference amorphous model of GaAs generated in this work. The inset gives the time evolution of the HOMO (black), the LUMO (black), the instantaneous Fermi level $\epsilon_F$ (green), and the reference level $\epsilon_{ref}$ (cyan). The energies are referred to the valence band maximum (VBM).

molecular orbital (HOMO) and the lowest unoccupied molecular orbital (LUMO), from which we extract an average HOMO-LUMO gap of 0.53 eV. This value agrees well with the corresponding gap of $\approx 0.6$ eV found in a previous first-principles study [39]. The Fermi level in our reference system is found to be located in the middle of the band gap, at 0.26 eV from the valence band maximum (VBM).

To perform constant-Fermi-level molecular dynamics, it is necessary to set the value of $\bar{\epsilon}_F$ with respect to the electronic structure of the evolving system. To this end, we adopted for alignment a common reference $\epsilon_{ref}$, which corresponds to the average single-particle energy level in the deepest band of the density of states. This band approximately extends from $-8.5$ to $-13.5$ eV when referred to the position of the VBM in the reference system (see Fig. 2). It originates from $4s$ As orbitals and does not overlap with the other bands for all the systems considered. This band represents a good choice for the alignment as it is only marginally affected by the presence of extra electrons or holes in states occurring close to the band edges. For the reference system, the energy level $\epsilon_{ref}$ exhibits very small fluctuations during the evolution as compared to those of the HOMO, the LUMO, and the instantaneous Fermi level (see Fig. 2). This further supports $\epsilon_{ref}$ as a reliable level for the alignment. In this work, we adopt this alignment and all the energy levels are referred to the VBM of the reference system.

Hence, we set the Fermi level at different positions with respect to the band edges during the molecular dynamics. Consequently, the system exchanges electrons with the
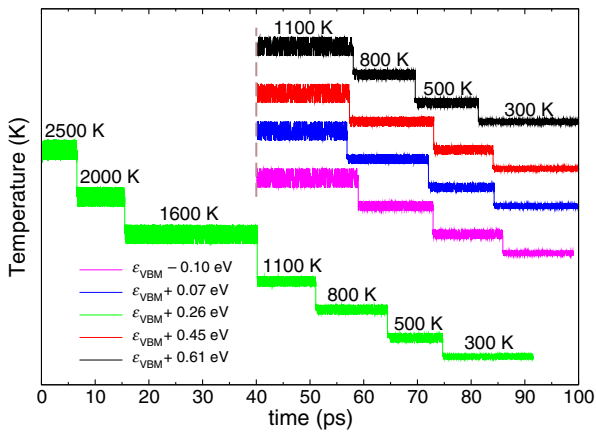


FIG. 1. Time evolution of the temperature during the quenching protocol used to generate the GaAs amorphous models at various Fermi levels, as indicated in the legend.

external reservoir and the atomic structure arranges accordingly. In this way, we can explore the dependence of the defect concentrations and the structure in general on the position of the preset Fermi level. We generate four amorphous systems by setting the target Fermi level at different energies. For the generation of each of these four systems, we start the constant-Fermi-level simulation from the last configuration of the liquid state equilibrated at $T = 1600$ K. As shown in Fig. 1, we adopt a quenching protocol similar to the one used for the reference system. With the adopted alignment, the Fermi levels of these four systems are at $-0.10$, $+0.07$, $+0.45$, and $+0.61$ eV. Figure 3 shows the time evolution of the Fermi level and of the electronic charge during the molecular dynamics of the amorphous systems at 300 K.

Compared to the Fermi level of the reference system [Fig. 3(c)], we generate two models with Fermi levels at higher (0.45 eV) and lower (0.07 eV) energy in the band gap. We also choose Fermi levels degenerate with either the valence ($-0.10$ eV) or the conduction ($+0.61$ eV) band to simulate conditions of carrier degeneracy. In all cases, the instantaneous Fermi levels show stable fluctuations around



FIG. 3. Time evolution of the instantaneous Fermi level $\epsilon_F$ (green) and of the total electronic charge (in units of $e$) in the system (red) during the constant-Fermi-level molecular dynamics of amorphous GaAs at 300 K. Panel (c) corresponds to the reference system produced without fixing the Fermi level ($\epsilon_F = 0.26$ eV). Panels (a), (b), (d), and (e) correspond to systems generated by setting the Fermi level $\bar{\epsilon}_F$ at $-0.10$, $+0.07$, $+0.45$, and $+0.61$ eV, respectively.

the target values during the molecular dynamics. For target values close to the VBM [Figs. 3(a) and 3(b)], the system releases electrons toward the reservoir. Correspondingly, the total charge of these systems becomes positive and stabilizes around $+16e$ and $+10e$ for the systems generated with $\bar{\epsilon}_F$ at $-0.10$ and 0.07 eV, respectively. On the other hand, setting the target Fermi level close to the CBM leads to extra electrons in the system. We find total electronic charges of about $-6e$ and $-12e$ for the simulations with $\bar{\epsilon}_F$ at 0.45 and 0.61 eV [Figs. 3(d) and 3(e)], respectively. In this way, we generate amorphous models representative of both n-type and p-type GaAs.

We observe that the concentration of extra electrons or holes reaches unrealistically high levels in our simulations, up to $+0.25e/$atom for extra holes and up to $-0.18e/$atom for extra electrons. This could be explained by the fact that charge addition in our systems is not opposed by Coulomb repulsion, due to the use of a uniform neutralizing background. Nevertheless, we expect the defect mechanisms occurring in response to the extra charge to be insightful.

## IV. ATOMIC STRUCTURE AND WANNIER-FUNCTION DECOMPOSITION

We are interested in identifying defective structures which we qualify as such in comparison to crystalline GaAs. In the following analysis, we focus on homopolar bonds which break the chemical order and on coordination defects which manifest as deviations from fourfold coordination. To this end, we carry out analyses based on both the atomic structure and a Wannier-function decomposition of the electronic structure. The latter is instrumental to properly identifying chemical bonds and occupied dangling bonds (lone pairs).

### A. Analysis of the atomic structure

In order to investigate the structural properties of the amorphous models of GaAs generated at various Fermi levels, we calculate the partial pair-correlation functions $g_{\alpha\beta}(r)$ with $\alpha$, $\beta = $ Ga or As (Fig. 4). The first peaks in $g_{GaGa}(r)$ and $g_{AsAs}(r)$ are located at about 2.50 Å and are indicative of the presence of homopolar Ga—Ga and As—As bonds, respectively. In the case of As-As correlations, the intensity of this peak exhibits a steady increase as the Fermi level moves from the conduction to the valence band, reflecting the presence of a higher concentration of As-As dimers for Fermi levels close to the VBM. For Ga-Ga correlations, the intensity of the first peak shows the opposite behavior. For Fermi levels moving closer to the VBM, this peak undergoes broadening until the first minimum is no longer discernable. This implies that the topology of the system is highly affected by the holes injected at these positions of the Fermi energy. For levels moving closer to the CBM, the first peak in $g_{GaGa}(r)$ becomes sharper and the formation of homopolar Ga-Ga is
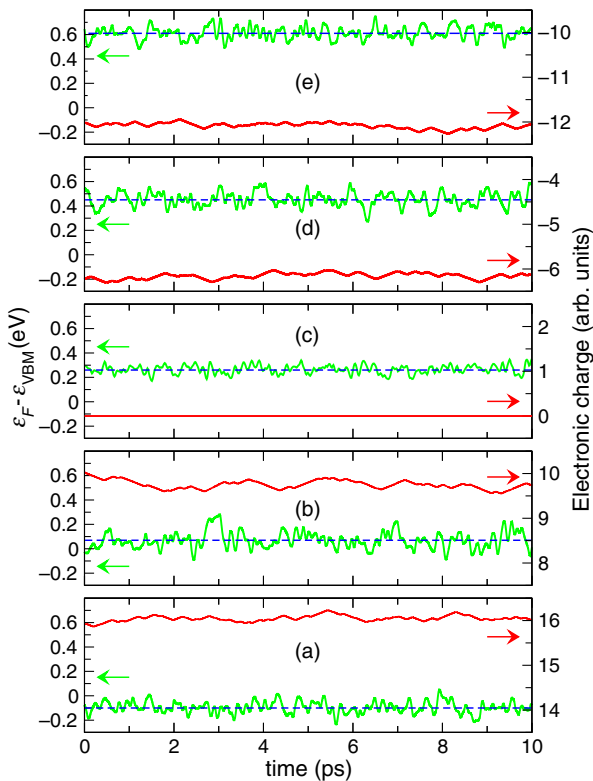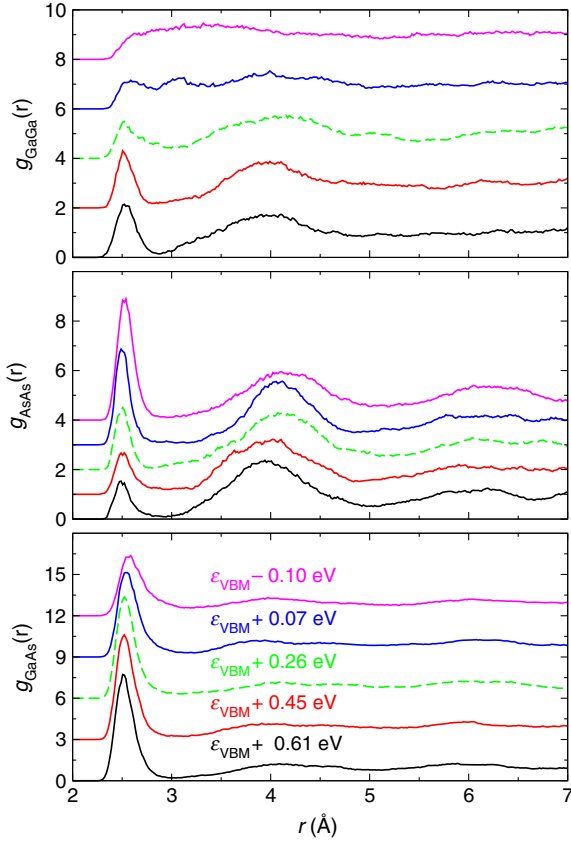
FIG. 4. Ga-Ga, As-As, and Ga-As partial pair-correlation functions of the amorphous models of GaAs generated at various Fermi levels. The results correspond to averages over 10 ps of molecular dynamics at a temperature of 300 K. The results for the neutral reference system are given by dashed lines.

favored. The modification of the local environment around the Ga atoms reflected by the Ga-Ga correlations is also mirrored in the Ga-As correlations. In particular, as the Fermi level approaches the CBM and the first peak in $g_{GaGa}(r)$ gets better defined, the first peak in $g_{GaAs}(r)$ becomes sharper and its intensity higher. This indicates that the creation of well-defined homopolar Ga—Ga bonds correlates with the chemical order in the system. In particular, the present results suggest that amorphous GaAs generated in $n$-type conditions exhibits a higher chemical order. More generally, the analysis of the partial pair-correlation functions shows that the atomic structures of the generated amorphous models depend on the position of the Fermi level in the band gap.

## B. Analysis based on Wannier functions

The centers ($W$) of maximally localized Wannier functions provide us with a compact real-space representation of the electron structure, which we can use to detect the chemical bonds and lone pairs. In this representation, a Wannier function corresponds to the localization of two electrons and its center $W$ gives its average position. Figure 5
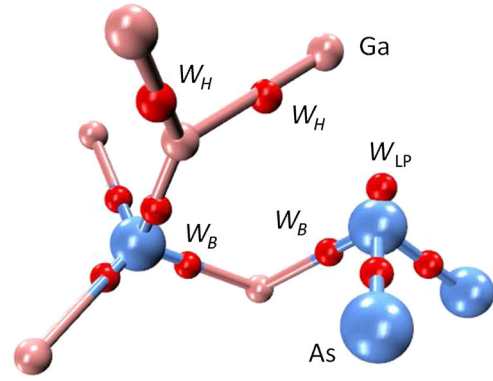


FIG. 5. Structural motif representative of the bonding environment in amorphous GaAs. Ga and As atoms are shown in pink and cyan, respectively. We also show the centers of maximally localized Wannier functions, labeled as $W$ (blue). Three different Wannier centers can be distinguished. The first type ($W_B$) refers to regular Ga—As bonds. The second type ($W_H$) refers to homopolar Ga—Ga or As—As bonds. The third type ($W_{LP}$) indicates lone pairs of valence electrons, i.e., occupied dangling bonds, which do not participate to the formation of chemical bonds but remain localized in the vicinity of the atoms.

illustrates a typical structural motif in amorphous GaAs, in which the location of representative Wannier centers is highlighted. Three Wannier centers can be distinguished. The first type of Wannier center ($W_B$) pertains to regular heteropolar Ga—As bonds analogous to those occurring in crystalline GaAs. The second type of Wannier centers ($W_H$) corresponds to homopolar linkages and they are generally found close to the middle of Ga—Ga or As—As bonds. The third type of Wannier centers ($W_{LP}$) corresponds to lone pairs attached to either Ga and As atoms (i.e., occupied dangling bonds) and they do not participate in the chemical bonding.

We compute the Wannier centers for all our structures and determine the resulting pair-correlation functions $g_{AsW}(r)$ and $g_{GaW}(r)$ (Fig. 6). For As-$W$ correlations, one can distinguish three main features [27,31], which arise from $W_{LP}$, $W_B$, and $W_H$ with increasing distance. As the Fermi level moves towards higher energies, the intensity of As-$W_{LP}$ correlations increases, while that of As-$W_H$ correlations decreases. This observation is consistent with the expected behavior of As-As dimer-DB defects at GaAs surfaces and interfaces [27,35]. For Ga-$W$ correlations, the $W$ centers give similar features, corresponding to $W_{LP}$, $W_H$, and $W_B$ with increasing distances. The intensity of Ga-$W_{LP}$ and Ga-$W_H$ correlations shows an opposite behavior for variation of the Fermi level. Specifically, the number of lone pairs diminishes and the number of homopolar Ga—Ga bonds grows as the Fermi level moves towards the CBM. For both As-$W$ and Ga-$W$ correlations, the feature corresponding to regular Ga—As bonds acquires higher intensity when the Fermi level is set close to the CBM. These findings agree with the trends observed in
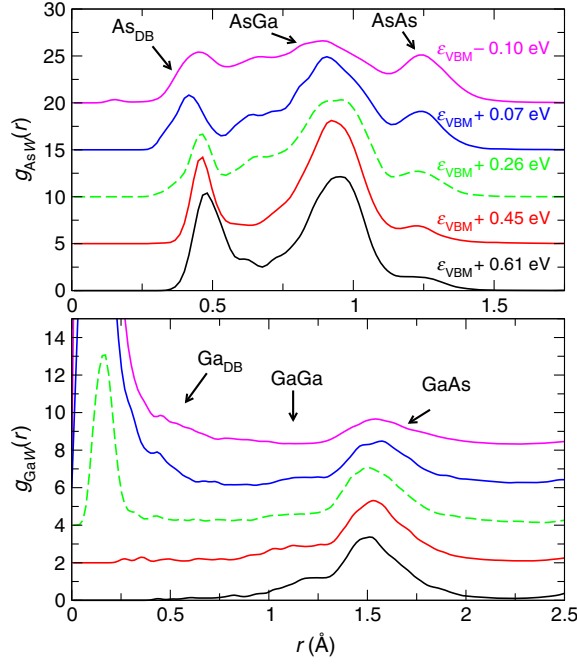
FIG. 6.   Correlation functions $g_{AsW}(r)$ and $g_{GaW}(r)$ between As and $W$ centers (upper panel) and between Ga and $W$ centers (lower panel), respectively, for the amorphous models evolving at 300 K. The various curves are labeled with their corresponding Fermi energy.

Fig. 4. The formation of a significant fraction of As dangling bonds and Ga homopolar bonds is inferred for Fermi energies in the vicinity of the CBM. These defects are supplanted by As homopolar bonds and Ga dangling bonds, as the Fermi level moves toward the VBM.

## V. IDENTIFICATION OF DEFECTS

With the objective of providing a description of the local environment, we adopt the following definitions for chemical and dangling bonds. It is convenient to first identify the lone pairs. For this purpose, we take the $W$ centers which are located at shorter distances than the first minimum in $g_{GaW}(r)$ or $g_{AsW}(r)$, depending on the considered atomic species. Next, among the remaining $W$ centers, heteropolar and homopolar bonds are assigned when a $W$ center is shared between two atoms of different or alike atomic species. In these assignments, we allow for a tolerance on the bond lengths, according to the inequality $r_{W\alpha} + r_{W\beta} - r_{\alpha\beta} < 0.25$ Å, where $\alpha$ and $\beta$ refer to Ga or As atoms. In this way, all the $W$ centers could be assigned to either lone pairs or atomic bonds.

Using the bonds defined in this way, we determine the coordination numbers of As and Ga atoms for all the amorphous models generated in this work (Fig. 7). When the Fermi level is set in the vicinity of the VBM, the Ga atoms are found to be mainly fourfold coordinated, but a substantial fraction of undercoordinated atoms subsists
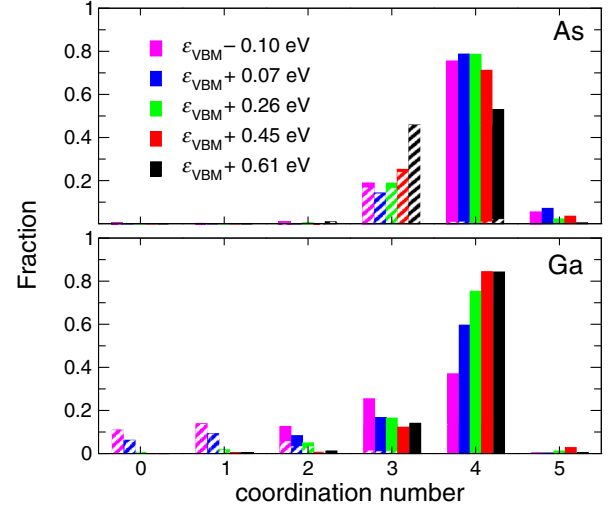


FIG. 7.   Distribution of coordination numbers $\ell$ for As and Ga atoms in the amorphous models of GaAs generated in this work. When the accounted atoms carry at least one lone pair, their contribution is shaded.

($\ell = 0$, 1, 2, and 3). The occurrence of the coordination number $\ell = 0$ for Ga atoms should be considered as an artifact associated with the adopted definition. This situation only occurs in low proportions, and thereby does not affect the overall validity of our analysis. For the majority fourfold and threefold coordinated Ga atoms, we essentially do not record any atoms carrying lone pairs as expected on the basis of electronegativity. Fivefold coordination only occurs in negligible amounts. As the Fermi level moves toward the CBM, the fraction of undercoordinated Ga atoms is suppressed in favor of fourfold coordinated ones. This detailed behavior underlies the trends observed in the Ga-Ga correlations shown in Fig. 4. As far as As atoms are concerned, fourfold coordination is dominant along with a substantial fraction of threefold coordination. When the Fermi level moves from the VBM to CBM, the fourfold coordination drops while the threefold coordination concurrently increases. We remark that essentially all of the threefold coordinated As atoms carry a lone pair. Fivefold coordinated As atoms occur in limited proportions, reaching at most 8%.

To follow the fractions of the main defective structures as a function of the preset Fermi level, it is convenient to include the unoccupied dangling bonds in the analysis. Wannier functions only provide information concerning the occupied states, but one can rely on the following rational. We first focus on the As atoms, for which the Wannier-function decomposition reveals dangling bonds in the form of lone pairs. Excluding the relatively small fraction of fivefold coordinated atoms, we remark that most of the other As atoms are either fourfold coordinated without carrying any lone pair or threefold coordinated with a single lone pair. This establishes a clear preference for fourfold hybridization in amorphous GaAs, mirroring the bonding in the parent

crystalline phase. Turning to Ga atoms, it is therefore reasonable to assume that such a fourfold hybridization is preserved. We thus assign unoccupied dangling bonds for each Ga atom on the basis of its coordination number and of its number of lone pairs. In this way, the fractions of atoms with homopolar and heteropolar bonds along with those with occupied and unoccupied dangling bonds can be inferred. Except for the fivefold coordinated atoms, this counting is normalized to account for the fourfold hybridization per atom.

In Fig. 8, we give the fractions of Ga and As atoms involved in heteropolar and homopolar bonds and carrying occupied and unoccupied dangling bonds as a function of the preset Fermi level. Focusing on the majority Ga—As bonds, we first remark that the chemical order is mostly favored when the Fermi level is set in the upper half of the band gap, in agreement with the description inferred from the study of Ga-As correlations in Fig. 4. The analysis for the As atoms reveals that the fraction of As—As homopolar bonds shows a steady decrease as the Fermi level moves from the VBM toward the CBM, while the fraction of the occupied As dangling bonds shows the opposite evolution. The conversion of As-As dimers into occupied As dangling bonds, i.e., the reaction

$$As - As + 2e^- \rightarrow 2DB_{As}^{\bullet}, \tag{3}$$

has previously been identified as the key mechanism to explain Fermi-level pinning in GaAs systems [27,31,35,36].
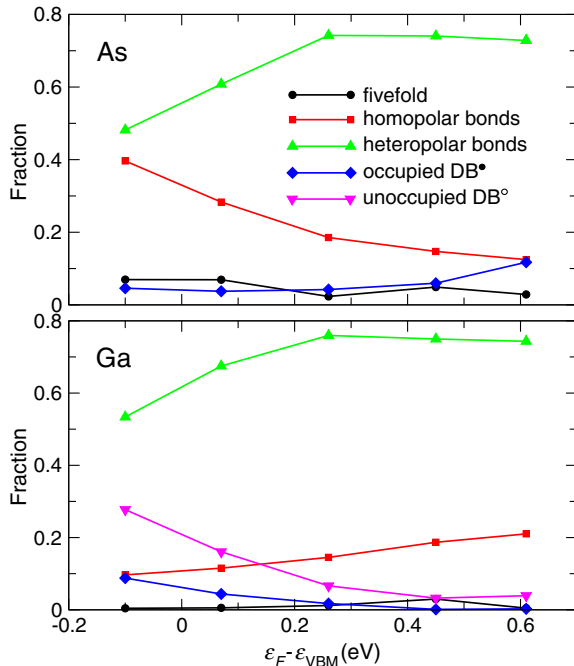


FIG. 8. Fractions of Ga and As atoms involved in heteropolar and homopolar bonds and carrying occupied and unoccupied dangling bonds as a function of the preset Fermi level. The results are obtained under the assumption of fourfold hybridization. The fractions of fivefold coordinated atoms are displayed separately.

We remark that in the present scheme, the key features of this conversion are directly captured through computer simulations without the necessity of any prior knowledge of the relevant defect.

For the Ga atoms, we observe that the fraction of homopolar bonds increases with Fermi energy. This trend is accompanied with a reduction of the fraction of unoccupied dangling bonds and, to a lesser extent, of occupied ones. This clearly reveals the following reaction mechanism:

$$Ga - Ga \rightarrow 2DB_{Ga}^{\circ} + 2e^-. \tag{4}$$
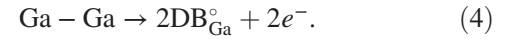
This mechanism might lead to a defect level in the band gap. However, at interfaces relevant for microelectronic devices, GaAs is generally in contact with excess oxygen, which preferentially oxidizes the Ga—Ga bonds, thereby passivating this defect. Nevertheless, the identification of this mechanism highlights once more the potential of the present computer-aided scheme in the identification of semiconductor defects.

To illustrate the possibility of providing a deeper description of the network of amorphous GaAs upon the conversion of As-As homopolar linkages into As lone pairs, we analyze in Fig. 9 the composition of the first-neighbor shell around the As atoms. For Fermi levels set in the vicinity of the VBM, the system shows a high fraction of As-As$_2$Ga$_2$ (37%) and As-AsGa$_3$ (22%) motifs consistent with the high concentration of As—As homopolar bonds (cf. Fig. 8). As the Fermi level moves to midgap ($\bar{\varepsilon}_F = 0.26$ eV), the frequency of As-As$_2$Ga$_2$ structural motifs diminishes favoring the appearance of As-Ga$_4$ and As-AsGa$_3$ motifs, in which As—As bonds are replaced by Ga—As bonds. For Fermi levels set at higher energies (0.45 and 0.61 eV), a second structural transition can be discerned involving the formation of lone pairs represented by As-Ga$_3 W_{LP}$ motifs at the expense of As-AsGa$_3$, As-As$_2$Ga$_2$, and As-Ga$_4$ motifs. These observations provide insight into the structural
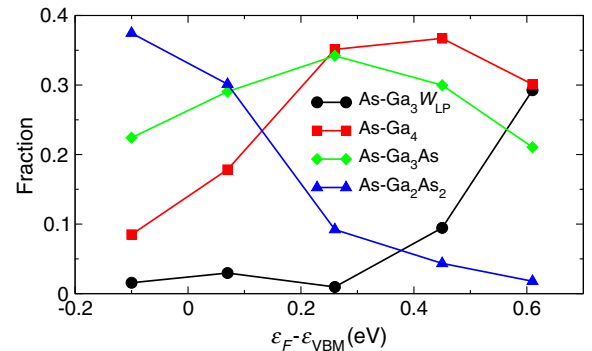


FIG. 9. Fractions of most abundant As structural motifs as a function of the preset Fermi level. The As atoms are distinguished by the composition of the first-neighbor shell, which might also include a lone pair ($W_{LP}$).

transformations which govern the conversion of As—As homopolar bonds into As dangling bonds.

## VI. CONCLUSIONS

Inspired from experimental studies on semiconductors, in which the Fermi level is controlled during growth, we explore in this work the use of constant-Fermi-level *ab initio* molecular dynamics as a computer-aided simulation technique to investigate the occurrence of defects in semiconductor materials. Our approach is free from human bias and does not require the prior knowledge of the defect structures. Using this simulation technique, we demonstrate that it is possible to generate amorphous models, for which the Fermi level is fixed at a preset value. The system spontaneously favors the formation of defects that show higher stability at the selected Fermi level. Hence, the basic principle of our scheme is that the defect population undergoes modification upon crossing defect charge transition levels. In particular, this offers the possibility of achieving computer-generated semiconductor structures representative of *n*-type or *p*-type semiconductors.

We validate our technique in the case of amorphous GaAs, as a model of the structure at GaAs interfaces. Fixing the Fermi level at various energies, we first generate four amorphous models through a melt-quench simulation protocol. We achieve stable molecular dynamics both when the Fermi level lies within the band gap or is degenerate with the band edges. For comparison, we also generate a reference amorphous model without controlling the Fermi energy. Next, we carefully inspect the structural and bonding properties of the achieved models. The analysis of the partial pair-correlation functions allows us to highlight structural differences between the models in terms of Ga—Ga, As—As, and Ga—As bonds. To investigate the variations in the chemical bonding and the local environment, we employ a Wannier-function decomposition. This real-space representation of the electronic structure allows us to distinguish between heteropolar bonds, homopolar bonds, and lone pairs. In this way, we are able to follow the evolution of the fraction of defective structures as the Fermi level moves across the band gap. Consequently, the evolution trends resulting from this analysis allow us to infer relevant transformations occurring between defective structures, thus providing an indication of the charge trapping mechanisms operative in the semiconductor system. For instance, we observe a clear anticorrelation between the occurrence of As—As homopolar bonds and As dangling bonds as the Fermi level varies across the band gap. This clearly hints at the interconversion of these two defective structures upon charge exchange. Similarly, the correlated variation of the fractions of Ga dangling bonds and Ga—Ga homopolar bonds suggests the occurrence of a charge transition level involving these two defective structures. This application illustrates how the present scheme is able to reveal detailed charge exchange mechanisms, which could previously only be accessed through educated guesses or trial-and-error procedures.

In conclusion, we demonstrate the effectiveness of the constant-Fermi-level *ab initio* molecular dynamics technique in revealing charge trapping mechanisms associated with defect levels in the band gap. The method is expected to serve as an invaluable tool towards the identification and passivation of undesired defects in semiconductor compounds. Especially when common practices based on physical intuition have failed, the present scheme constitutes an alternative computer-aided search procedure, which is not subject to human bias.

---

[1] Paolo A. Gargini, The global route to future semiconductor technology, IEEE Circuits Devices Mag. **18**, 13 (2002).

[2] Juan Antonio Carballo, Wei Ting Jonas Chan, Paolo A. Gargini, Andrew B. Kahng, and Siddhartha Nath, in *Proceedings of the 32nd IEEE International Conference on Computer Design (ICCD), 2014* (IEEE, New York, 2014), pp. 139–146.

[3] Ling Xia, J. Brad Boos, Brian R. Bennett, Mario G. Ancona, and Jesus A. del Alamo, Hole mobility enhancement in $In_{0.41}Ga_{0.59}Sb$ quantum-well field-effect transistors, Appl. Phys. Lett. **98**, 053505 (2011).

[4] Y. Xuan, Y. Q. Wu, and P. D. Ye, High-performance inversion-type enhancement-mode InGaAs MOSFET with maximum drain current exceeding 1 A/mm, IEEE Electron Device Lett. **29**, 294 (2008).

[5] Jesús A. Del Alamo, Dimitri A. Antoniadis, Jianqiang Lin, Wenjie Lu, Alon Vardi, and Xin Zhao, Nanometer-scale III-V MOSFETS, IEEE J. Electron Devices Soc. **4**, 205 (2016).

[6] K. Rajagopalan, J. Abrokwah, R. Droopad, and M. Passlack, Enhancement-mode GaAs *n*-channel MOSFET, IEEE Electron Device Lett. **27**, 959 (2006).

[7] K. Rajagopalan, R. Droopad, J. Abrokwah, P. Zurcher, P. Fejes, and M. Passlack, 1-$\mu$m enhancement mode GaAs n-channel MOSFETs with transconductance exceeding 250 ms/mm, IEEE Electron Device Lett. **28**, 100 (2007).

[8] Y. Sun, E. W. Kiewra, S. J. Koester, N. Ruiz, A. Callegari, K. E. Fogel, D. K. Sadana, J. Fompeyrine, D. J. Webb, J. P. Locquet, M. Sousa, R. Germann, K. T. Shiu, and S. R. Forrest, Enhancement-mode buried-channel, IEEE Electron Device Lett. **28**, 473 (2007).

[9] M. Hong, J. Kwo, A. R. Kortan, J. P. Mannaerts, and A. M. Sergent, Epitaxial cubic gadolinium oxide as a dielectric for gallium arsenide passivation, Science 283, 1897 (1999).

[10] Guy Brammertz, H. C. Lin, Koen Martens, David Mercier, Sonja Sioncke, Annelies Delabie, Wei E Wang, Matty Caymax, Marc Meuris, and Marc Heyns, Capacitance-voltage characterization of GaAs-$Al_2O_3$ interfaces, Appl. Phys. Lett. 93, 183504 (2008).

[11] Ted H. Yu, Liang Yan, Wei You, Ramesh B. Laghumavarapu, Diana Huffaker, and Christian Ratsch, The effect of passivation on different GaAs surfaces, Appl. Phys. Lett. 103, 173902 (2013).

[12] Zachary Bryan, Marc Hoffmann, James Tweedie, Ronny Kirste, Gordon Callsen, Isaac Bryan, Anthony Rice, Milena Bobea, Seiji Mita, Jinqiao Xie, Zlatko Sitar, and Ramn Collazo, Fermi level control of point defects during growth of Mg-doped GaN, J. Electron. Mater. 42, 815 (2013).

[13] Zachary Bryan, Isaac Bryan, Benjamin E. Gaddy, Pramod Reddy, Lindsay Hussey, Milena Bobea, Wei Guo, Marc Hoffmann, Ronny Kirste, James Tweedie, Michael Gerhold, Douglas L. Irving, Zlatko Sitar, and Ramn Collazo, Fermi level control of compensating point defects during metal-organic chemical vapor deposition growth of Si-doped AlGaN, Appl. Phys. Lett. 105, 222101 (2014).

[14] P. Reddy, M. P. Hoffmann, F. Kaess, Z. Bryan, I. Bryan, M. Bobea, A. Klump, J. Tweedie, R. Kirste, S. Mita, M. Gerhold, R. Collazo, and Z. Sitar, Point defect reduction in wide bandgap semiconductors by defect quasi Fermi level control, J. Appl. Phys. 120, 185704 (2016).

[15] Marc P. Hoffmann, James Tweedie, Ronny Kirste, Zachary Bryan, Isaac Bryan, Michael Gerhold, Zlatko Sitar, and Ramón Collazo, in *Point Defect Management in GaN by Fermi-Level Control during Growth*, SPIE Proceedings Vol. 8986 (SPIE–International Society for Optical Engineering, Bellingham, WA, 2014).

[16] Nicéphore Bonnet, Tetsuya Morishita, Osamu Sugino, and Minoru Otani, First-Principles Molecular Dynamics at a Constant Electrode Potential, Phys. Rev. Lett. 109, 266101 (2012).

[17] Assil Bouzid and Alfredo Pasquarello, Redox levels through constant Fermi-level *ab initio* molecular dynamics, J. Chem. Theory Comput. 13, 1769 (2017).

[18] John Robertson, Model of interface states at III-V oxide interfaces, Appl. Phys. Lett. 94, 152104 (2009).

[19] Darby L. Winn, Michael J. Hale, Tyler J. Grassman, Jonathan Z. Sexton, Andrew C. Kummel, Matthias Passlack, and Ravi Droopad, Electronic properties of adsorbates on GaAs (001)-c $(2 \times 8)/(2 \times 4)$, J. Chem. Phys. 127, 134705 (2007).

[20] K. Laasonen, Risto M. Nieminen, and Martti J. Puska, First-principles study of fully relaxed vacancies in GaAs, Phys. Rev. B 45, 4122 (1992).

[21] J. T. Schick, C. G. Morgan, and P. Papoulias, First-principles study of as interstitials in GaAs: Convergence, relaxation, and formation energy, Phys. Rev. B 66, 195302 (2002).

[22] Hannu Pekka Komsa and Alfredo Pasquarello, Dangling bond charge transition levels in AlAs, GaAs, and InAs, Appl. Phys. Lett. 97, 191901 (2010).

[23] John Robertson and L. Lin, Bonding principles of passivation mechanism at III-V-oxide interfaces, Appl. Phys. Lett. 99, 222906 (2011).

[24] Giacomo Miceli and Alfredo Pasquarello, Accurate determination of charge transition levels of the As-As dimer defect at GaAs/oxide interfaces through hybrid functionals, Appl. Phys. Lett. 103, 041602 (2013).

[25] Weichao Wang, Ka Xiong, Robert M Wallace, and Kyeongjae Cho, First-principles study of initial growth of GaXO layer on GaAs-$\beta$2 $(2 \times 4)$ surface and interface passivation by F, J. Appl. Phys. 110, 103714 (2011).

[26] Giacomo Miceli and Alfredo Pasquarello, Defect levels at $GaAs/Al_2O_3$ interfaces: As–As dimer vs. Ga dangling bond, Appl. Surf. Sci. 291, 16 (2014).

[27] Davide Colleoni, Giacomo Miceli, and Alfredo Pasquarello, Origin of Fermi-level pinning at GaAs surfaces and interfaces, J. Phys. Condens. Matter 26, 492202 (2014).

[28] J. Robertson, Y. Guo, and L. Lin, Defect state passivation at III-V oxide interfaces for complementary metal-oxide-semiconductor devices, J. Appl. Phys. 117, 112806 (2015).

[29] S. Pöykkö, Martti J. Puska, M. Alatalo, and Risto M. Nieminen, Metastable defect complexes in GaAs, Phys. Rev. B 54, 7909 (1996).

[30] M. J. Caldas, J. Dabrowski, A. Fazzio, and M. Scheffler, Anion-Antisite-like Defects in III-V Compounds, Phys. Rev. Lett. 65, 2046 (1990).

[31] Davide Colleoni and Alfredo Pasquarello, Interfacial Ga-As suboxide: Structural and electronic properties, Appl. Phys. Lett. 107, 031605 (2015).

[32] Davide Colleoni and Alfredo Pasquarello, Oxygen defects in GaAs: A hybrid functional study, Phys. Rev. B 93, 125208 (2016).

[33] A. Stroppa, X. Duan, M. Peressi, D. Furlanetto, and S. Modesti, Computational and experimental imaging of Mn defects on GaAs (110) cross-sectional surfaces, Phys. Rev. B 75, 195335 (2007).

[34] T. Mattila and Risto M. Nieminen, *Ab initio* study of oxygen point defects in GaAs, GaN, and AlN, Phys. Rev. B 54, 16676 (1996).

[35] Davide Colleoni, Giacomo Miceli, and Alfredo Pasquarello, Fermi-level pinning through defects at GaAs/oxide interfaces: A density functional study, Phys. Rev. B 92, 125304 (2015).

[36] Davide Colleoni and Alfredo Pasquarello, Amphoteric defects in GaAs leading to Fermi-level pinning: A hybrid functional study, Microelectron. Eng. 109, 50 (2013).

[37] Nigel J. Shevchik and William Paul, The structure of tetrahedrally coordinated amorphous semiconductors, J. Non-Cryst. Solids 13, 1 (1973).

[38] F. S. Aguirre Tostado, M. Milojevic, K. J. Choi, H. C. Kim, C. L. Hinkle, E. M. Vogel, J. Kim, T. Yang, Y. Xuan, P. D. Ye, and R. M. Wallace, S passivation of GaAs and band bending reduction upon atomic layer deposition of $HfO_2/Al_2O_3$ nanolaminates, Appl. Phys. Lett. 93, 061907 (2008).

[39] E. Fois, Annabella Selloni, G. Pastore, Q. M. Zhang, and Roberto Car, Structure, electronic properties, and defects of amorphous gallium arsenide, Phys. Rev. B 45, 13378 (1992).

[40] Hyangsuk Seong and Laurent J. Lewis, Tight-binding molecular-dynamics study of density-optimized amorphous GaAs, Phys. Rev. B 53, 4408 (1996).

[41] C. Molteni, L. Colombo, and L. Miglio, Structural properties of liquid and amorphous GaAs by tight-binding molecular dynamics, Europhys. Lett. **24,** 659 (1993).

[42] J. P. Perdew, K. Burke, and M. Ernzerhof, Generalized Gradient Approximation Made Simple, Phys. Rev. Lett. **77,** 3865 (1996); Erratum, Phys. Rev. Lett. **78,** 1396(E) (1997).

[43] N. Troullier and J. L. Martins, Efficient pseudopotentials for plane-wave calculations, Phys. Rev. B **43,** 1993 (1991).

[44] M. L. Theye, A. Gheorghiu, and H. Launois, Investigation of disorder effects in amorphous GaAs and GaP by EXAFS, J. Phys. C **13,** 6569 (1980).

[45] C. Ascheron, A. Schindler, R. Flagmeyer, and G. Otto, A comparative study of swelling, strain and radiation damage of high-energy proton-bombarded GaAs, GaP, InP, Si and Ge single crystals, Nucl. Instrum. Methods Phys. Res., Sect. B **36,** 163 (1989).

[46] C. M. H. Driscoll, A. F. W. Willoughby, J. B. Mullin, and B. W. Straughan, in *Gallium Arsenide and Related Compounds*, edited by J. Bok, IOP Conference Proceedings No. 24 (Institute of Physics and Physical Society, London, 1975), p. 275.

[47] Hannu Pekka Komsa, Tapio T. Rantala, and Alfredo Pasquarello, Finite-size supercell correction schemes for charged defect calculations, Phys. Rev. B **86,** 045112 (2012).